

Electronic and optical properties of transition metals doped ZnS: first principles study

D. E. AIMOUCHE^{a*}, S. MESKINE^a, A. ZAOUT^b, A. BOUKORTT^a

^aLaboratoire d'Elaboration et Caractérisation Physico Mécanique et Métallurgique des Matériaux (ECP3M), Département de Génie Electrique, Faculté des Sciences et de la Technologie, Université Abdelhamid Ibn Badis de Mostaganem, 27000 Mostaganem, Algeria

^bLaboratoire de Physique Computationnelle des Matériaux, Université Djillali Liabès de Sidi Bel-Abbès, Sidi Bel-Abbès 22000, Algeria.

Electronic and optical properties of TM-doped zinc sulphide (TM=Ti, Co, Ni) were calculated with the FP-LAPW method by using the LSDA and LSDA+ U approximations. In this study, we used the cubic structure of ZnS doped with a 6.25% concentration of transition metals. Our computed electronic band structure and density of states show the semiconducting behavior of TM-doped ZnS. We found $U=10$ eV the adequate value to obtain the filled d - eg states of titanium, and Ti doped ZnS acts as a semiconductor compound. $U=3.3$ eV applied to Co $3d$ states gives good results for exchange couplings close to the previous work, and Co doped ZnS shows a semiconducting behavior. $U=6.4$ eV is applied to nickel $3d$ states, and Ni doped ZnS keeps its half-metallic character compared to the calculation without Hubbard. In contrast, we used the Jahn Teller effect to break up the Ni- d_{2g} level lying around the Fermi level, and Ni doped ZnS changed to semiconductor compound. Furthermore, the optical properties such as the real and imaginary part of dielectric function and the absorption coefficients show new transition peaks after doping ZnS with TM impurity. The energy band gap of ZnS was found to be decreased by doping with transition metal impurity. That tendency agrees well with the available experimental data.

(Received March 2, 2016; accepted November 25, 2016)

Keywords: Optoelectronic, Magnetic, Half-metallic, LSDA+ U

1. Introduction

Diluted magnetic semiconductors (DMSs) and half-metal behaviors in $3d$ transition metals doped II-IV semiconductors have attracted much attention recently as potential candidates for use in spintronics applications and magneto-optics based devices, DMSs are semiconductors in which some cations can be substituted by the transition metals (TM) ions. However, Zinc Sulphide (ZnS) is II-VI group semiconductor with a large direct band gap in the near UV region. The wide band gap of the material makes it suitable for use in optoelectronic devices. ZnS was doped with different compounds in previous experimental works, such as, cadmium and manganese (Cd/Mn) [1], copper (Cu) [2], chromium (Cr) [3], cobalt (Co) [4] Iron (Fe)[5]. It has been reported for these impurities a good enhancement on the optical properties of compounds. Furthermore, there are theoretical works on transition metal doped ZnS such as nickel (Ni) [6], manganese (Mn) [7], cobalt (Co) [8], titanium (Ti) [9]. These transition metals change the electronic and optical properties of ZnS to achieve a good conception of optoelectronics devices. ZnS was used for different applications such as light-emitting diodes (LEDs), electroluminescence devices, sensors, lasers, solar cells etc. Generally, magnetic moment originates from $3d$ orbital of transition metals. Accordingly, it was possible to study the spin-phenomenon of semiconductor alloys. Y. Chen et al [9]

reported that the magnetic moment comes mainly from spin polarized Ti atoms in ZnS. However, M.S. Akhtar et al. studied the Fe doped ZnS and the result indicates that the compound may be a promising half-metallic ferromagnetic material [5].

In this paper, we present the electronic structure of TM-doped ZnS to show the magnetic behavior of these compounds. We calculate the exchange couplings N_α and N_β to study the interaction between d -TM states and valence/conduction band of the host material. We check Hubbard U correction on the splitting of TM- $3d$ band. Furthermore, we present the optical properties of TM-doped ZnS such as the real part and the imaginary part of dielectric function, and the absorption coefficient. Our objectives in this work is to investigate the effect of TM doping on the optical properties such as optical transitions that provide information on emissions or absorption energy for various applications in the optoelectronics field, which will be explained in details.

2. Method of calculation

The Density Functional Theory (DFT) with Full Potential Linearized Augmented Plane Wave (FP-LAPW) and Local Spin density Approximation (LSDA) are used to calculate the electronic and optical properties of TM-doped ZnS. 3. We used the Hubbard parameter $U=6$ eV

applied to titanium $3d$ states [10]. The Hubbard $U=3.3$ eV and $U=6.4$ eV is applied to cobalt $3d$ states and nickel $3d$ states, respectively, taken from [11]. The optimized cubic structure of ZnS is containing 32 atoms, 16 atoms of Zn and 16 atoms of S. The $R_{MT} \cdot K_{max}$ is set to 7.0, where K_{max} is the plane wave cut-off and R_{MT} the smallest of all MT sphere radii. The Muffin-tin radii of Zn and S are 2.0, 1.8, respectively. We use 800 K-point in the irreducible Brillouin zone for TM concentration of 6.25% (6.25% TM). The TM doping on ZnS was performed by the substitution of one Zn atom by one TM atom. Therefore, the lattice parameter was obtained as follow $a=5.303\text{\AA}$, 5.340\AA , 5.290\AA , and $a=5.288\text{\AA}$, for pure ZnS, ZnS:Ti, ZnS:Co, and ZnS:Ni respectively. The lattice parameter of pure ZnS is in a good agreement with the other theoretical work [12] and experimental work [13]. However, it increases by doping with Ti element and it decreases by doping with Co and Ni elements, due to the larger ionic radius of Ti(1\AA) and smaller ionic radius of Co(0.79\AA) and Ni(0.83\AA) compared to that of Zn(0.88\AA) [13,14] (see in Fig. 1). Thus, the optimized energy as function of volume of TM- doped ZnS is presented in Fig. 2.

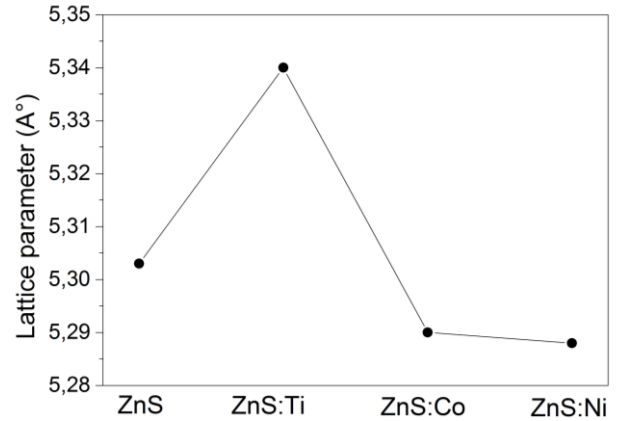


Fig. 1. The optimized lattice parameter of TM-doped ZnS

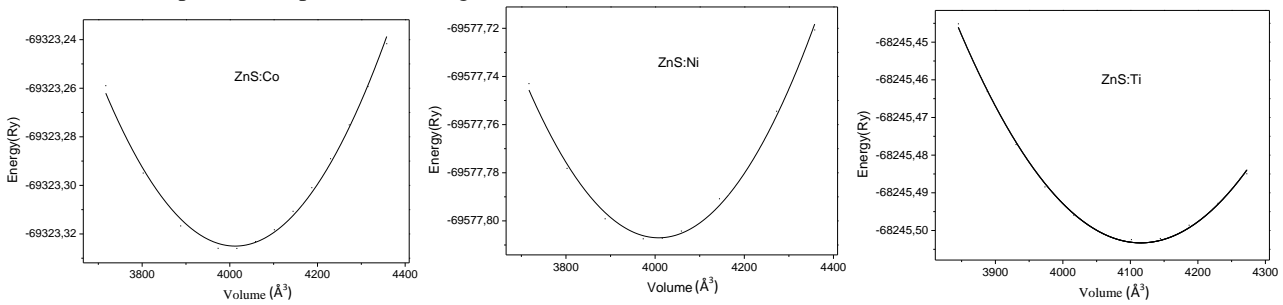


Fig. 2. The optimized energy of TM-doped ZnS

3. Results and discussions

3.1. Electronic properties

We present in Fig. 3. the spin-polarized band structure of TM-doped ZnS for spin up and spin down orientations. The conduction band minimum (CBM) and the valence band maximum (VBM) occur at gamma point of Brillouin zone, and this is good for optical properties. For LSDA calculation, both compound ZnS:Co and ZnS:Ni have half-metallic character. The other theoretical works show the same phenomenon using ab-initio calculations, where Co-doped ZnS was found to be half-metallic with minority spin being semiconducting and majority spin being metallic [15]. Xie *et al* [16] found the half metallic characteristic of Ni-doped ZnS with the majority spin being semi-conducting and the minority spin being metallic as it is confirmed by our calculations. This half-metallicity of both compounds induces $3.0\mu_B$ and $2.0\mu_B$ total magnetic moment for ZnS:Co and ZnS:Ni respectively, which comes mainly from Co and Ni elements (see in table 2). The spin polarization of conduction carriers indicates that Co and Ni doped ZnS

can be candidate for spin injection process [17,18]. On the other hand, for ZnS:Ti, the conduction band crosses the Fermi level for spin up channel, which indicates the metallic behavior, while the insulator character is presented in spin down channel, which means that ZnS:Ti have half-metallic character. The d - eg states around the Fermi level is partially filled, which is probably wrong corresponding to the spin configuration of Ti shown in Fig. 5. Thus, we found $U=10$ eV the adequate value to correct that deficiency and obtain the filled Ti- d - eg states (see in the bottom of Fig. 3.) Y. Chen *et al* [9] performed the calculation without Hubbard parameter and showed the Fermi level within Ti impurity bands, which found to be merged with the conduction band at higher carrier concentration. Moreover, we found that ZnS:Ni keeps its half-metallicity after introducing Hubbard parameter. In contrast, we used the Jahn-Teller effect within LSDA+ U functional (LSDA+ U + JT) to break up the d - $t2g$ lying around the Fermi level, subsequently, Ni doped ZnS change to semiconductor compound. A Jahn-Teller distortion which breaks cubic symmetry removed the degeneracy of the $t2g$ level.

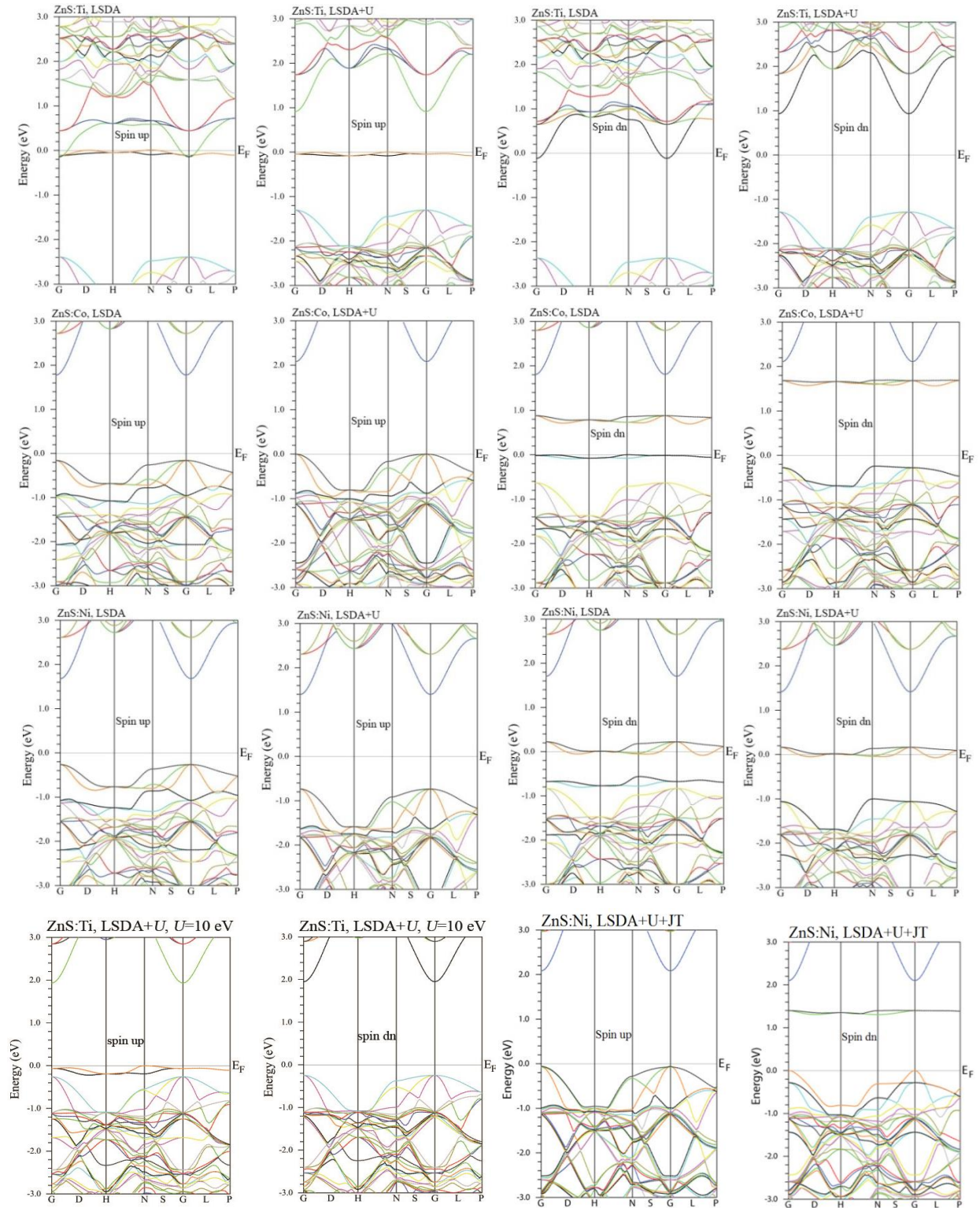


Fig. 3. The band structure of TM-doped ZnS with and without Hubbard correction plus Jahn Teller effect applied on ZnS:Ni

For ZnS:Co, the minority spin is being semiconducting when U term is added, maybe due to the Hubbard U correction applied to 3d-states of Cobalt.

The total and partial densities of states of TM-doped ZnS are depicted in Fig. 4. We correct the standard DFT LSDA Hamiltonian with an additional Hubbard interaction

term (LSDA+ U) [19]. LSDA calculation shows that TM-doped ZnS exhibit a half-metallic behavior by spin polarization around the Fermi level. From Fig. 4, we see that the transition metals introduce some energy levels in the band gap of the host material, these energy levels are dominated by 3d states of TM, and it proves certainly the

change in optoelectronic properties of the compounds. For ZnS:Ti, we see some levels of Ti impurity close to the minimum conduction band, which means that we have n-type doped material, and Ti dopants acts as donor in ZnS, which is confirmed by the other theoretical work [9]. Therefore, for ZnS:Co and ZnS:Ni, there are some energy levels of Co impurity close to the valence band maximum, which means that we have p-type doped material. The three transition metals show a spin polarization

phenomenon. For ZnS:Ti, the whole system have a half-metallic behavior, which was found in the band structure presentation. For ZnS:Co and ZnS:Ni compounds, it can be seen an appearance of an intra-band energy in spin down around Fermi level due to the transition metals elements. Both materials have a metallic character for spin down and an insulating character for spin up channel, which means that both compounds have half-metallic behavior.

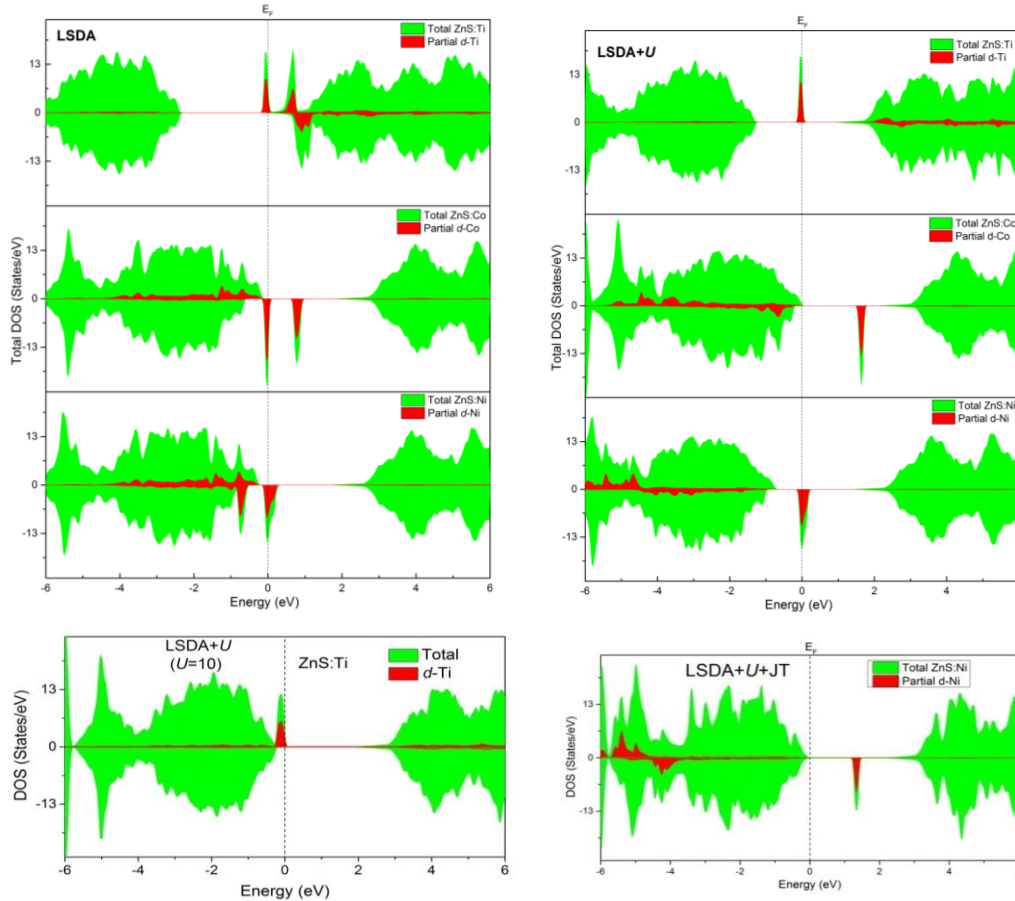


Fig. 4. Total and partial densities of states of TM-doped ZnS within LSDA and LSDA+U plus Jahn Teller effect applied on ZnS:Ni

In contrast, LSDA+U calculation is reported in the right side of Fig. 4. For ZnS:Ti, the valence band is shifted to the higher energy and breakup of the peak found previously in spin up channel around 1eV, but the second nearest peak remains around the Fermi level, which means that the compound remains its half-metallic behavior, which not corresponds to the spin configuration of $3d$ -Ti, where the d - eg level is completely filled. Thus, as it was explained by the band structure, $U=10$ eV was found sufficient to correct that deficiency. Moreover, for ZnS:Co, the valence band in spin down is shifted to the lower energy and breakup of the peak found previously around Fermi level, and the material became semiconductor as pure ZnS. While, ZnS:Ni acts as a semiconductor by inclusion of the Jahn-Teller effect. Furthermore, we understand the interaction between the magnetic moment created by TM impurities and the spin

of valence band using the following Hamiltonian equation [20]:

$$\hat{H} = N_{\beta} \sum_i S_i s_i \quad (1)$$

where N is the number of cations per volume, S_i is the spin operator of impurities, and s_i is the local spin operator of the valence band. The same Hamiltonian is for N_{α} . In addition, we calculated the values of spin exchange splitting energy ΔE_c and ΔE_v which are defined as $\Delta E_c = E_{c\downarrow} - E_{c\uparrow}$ and $\Delta E_v = E_{v\downarrow} - E_{v\uparrow}$ where $E_{c\downarrow}$ and $E_{c\uparrow}$ are the minimum conduction band of the minority-spin and the minimum conduction band of the majority-spin respectively.

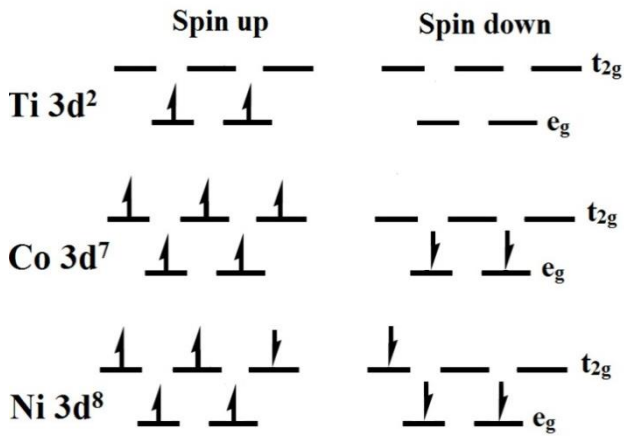


Fig. 5. The spin configuration of 3d-TM in the tetrahedral site

Tab 1. The energy valence band difference (ΔE_v), the energy conduction band difference (ΔE_c), and the sp - d exchange constant N_α and N_β .

		Ti	Co	Ni
ΔE_v (eV)	LSDA	0.026	-0.472	-0.556
	LSDA+U	0.020	-0.247	-0.327
	U=10 eV	0.012	-	-
	LSDA+U+JT	-	-	0.574
ΔE_c (eV)	LSDA	0.025	0.029	0.023
	LSDA+U	0.019	0.025	0.017
	U=10 eV	0.016	-	-
	LSDA+U+JT	-	-	-0.684
N_β (eV)	LSDA	0.416	-5.035	-8.896
	LSDA+U	0.320	-2.635	-5.232
	U=10 eV	0.193	-	-
	LSDA+U+JT	-	-	9.182
	Other work	-	-2.64 ^a	-
Other work	0.8 ^b	-2.2 ^b	-6.0 ^b	
N_α (eV)	LSDA	0.400	0.309	0.368
	LSDA+U	0.304	0.267	0.272
	U=10 eV	0.251	-	-
	LSDA+U+JT	-	-	-10.946
Other work	-	0.21 ^a	-	

^a [24]

^b [25]

The values of ΔE_c and ΔE_v are in table1. In addition, we calculated the p - d exchange constant N_β , which is the interaction between the valence band and $3d$ -states of the magnetic elements using the following formulas [21-23]:

$$N_\alpha = \frac{\Delta E_c}{x(S)} \quad (2)$$

$$N_\alpha = \frac{\Delta E_c}{x(S)} \quad (3)$$

where ΔE_c is the conduction band edge splitting and ΔE_v is the valence band edge splitting, x is the TM concentration,

and $\langle S \rangle$ is the half of magnetization per TM atoms. The calculated values of N_α and N_β for TM-doped ZnS are given in Table 1. For ZnS:Ti, we see that N_β and N_α values are positive, which means that the conduction band and the valence band states are behaving in the same manner, with ferromagnetic interaction between the doped holes-electrons and $3d$ states of Ti element. The ferromagnetic coupling in Ti-doped ZnS was explained in terms of p - d hybridization mechanism [9, 26]. The p - d exchange couplings of ZnS:Ti is in a good agreement with the previous work [25]. Furthermore, the N_β values of ZnS:Co and ZnS:Ni compounds are negative, while N_α values are positive. The negative values of N_β indicate the antiferromagnetic exchange interaction between the valence band states and $3d$ -band states of impurity. In this case, the effective potential for minority spin is more attractive than that of majority spin. The p - d hybridization in $3d$ -Co or $3d$ -Ni and $2p$ -S leads to the super-exchange interaction. This super-exchange mechanism is responsible for inducing anti-ferromagnetism in doped ZnS. By the other hand, it is clear that N_β values increased, and N_α values decreased by adding Hubbard parameter (see in table1). However, the exchange couplings of Co-doped ZnS agree well with the previous theoretical work [24]. The N_β value of Ni-doped ZnS also is in a good agreement with the previous theoretical work [25].

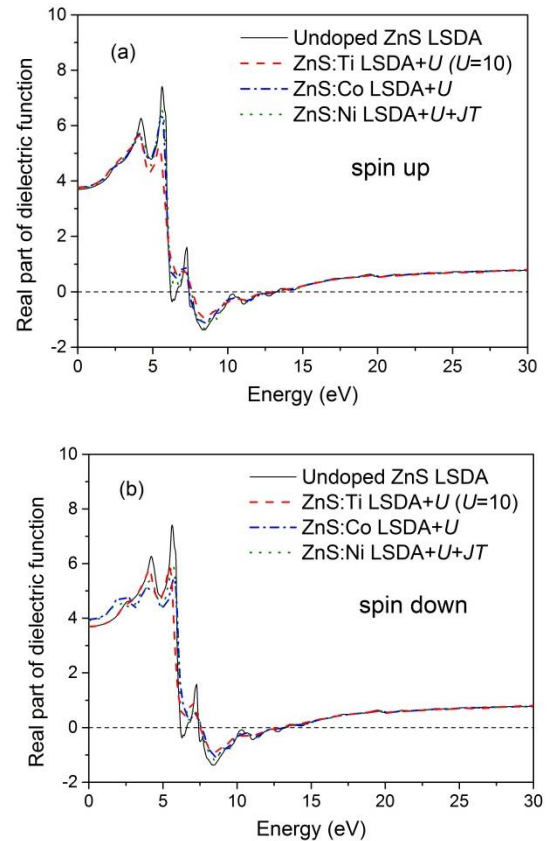


Fig. 6. The real part of dielectric function of TM-doped ZnS for (a) spin up and (b) spin down channels

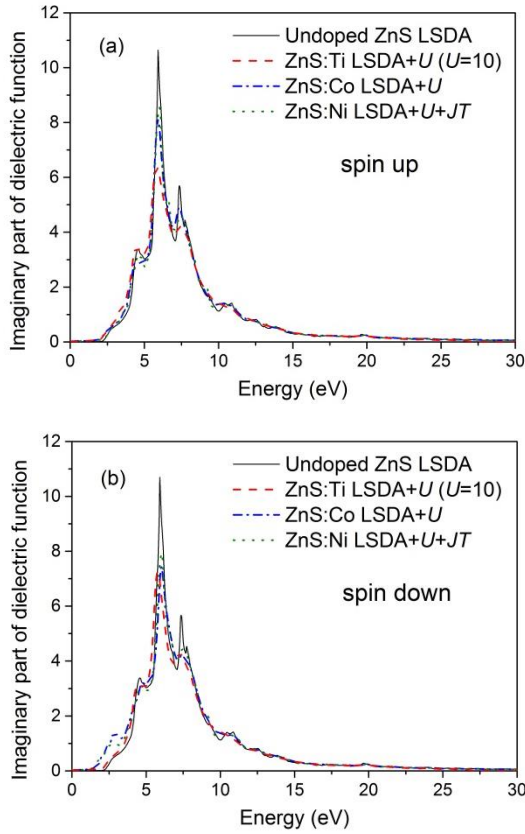


Fig. 7. The imaginary part of dielectric function of TM-doped ZnS for (a) spin up and (b) spin down channels

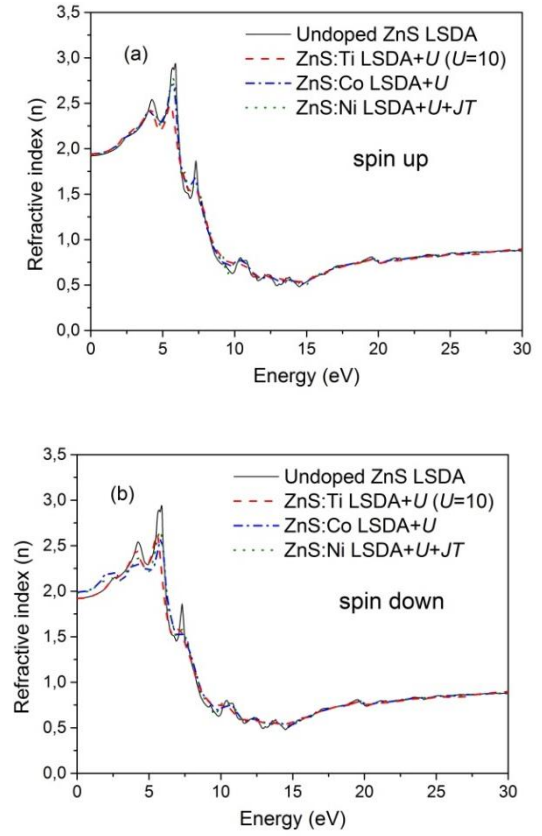


Fig. 8. The refractive index of TM-doped ZnS for (a) spin up and (b) spin down channels

Table 2. The total magnetic moment μ_{tot} , the local magnetic moment TM, and the energy band gap E_g of ZnS:TM calculated with LSDA and LSDA+U.

	Method	μ_{tot} (μ_B)	TM (μ_B)	μ_{int} (μ_B)
Ti	LSDA+U U=10 eV	2.001	1.581	0.359
Co	LSDA+U U=3.3 eV	3.000	2.363	0.330
Ni	LSDA+U+JT U=6.4 eV	1.998	1.609	0.172

3.2. Optical properties

The calculated magnetic moment of TM-doped ZnS is presented in Tab. 2. It is noticed that the total magnetic moment is dominated by the magnetic elements (Ti, Co, Ni). We can see that the local magnetic moment of the transition metals increased when U term is added. Furthermore, we present in Fig. 10. the plot of $(\alpha*hv)^2$ as function of energy to obtain the optical band gaps values of transition metals doped ZnS measurable by extrapolating the straight line to the $\alpha=0$. The optical band gap of TM-doped ZnS for the non-magnetic solution is presented in Tab. 3. The optical band gap values are 2.110 eV, 2.028 eV, 1.766 eV and 1.603 eV for undoped ZnS, ZnS:Ti, ZnS,Co and ZnS:Ni, respectively. It is noticed that the non-magnetic optical band gaps of ZnS decreases by doping with transition metals impurities compared to the pure ZnS (2.110eV).

That tendency agrees well with the available experimental data. However, in other experimental work, the gap was found to be decreased with increasing the concentration of Co in the host material ZnS [27]. The energy of the experimental gap Ni doped ZnS decreases with the increase of Ni concentration [28]. The energy gap of Ti doped ZnS also decreases with the incorporation of Ti in ZnS [29].

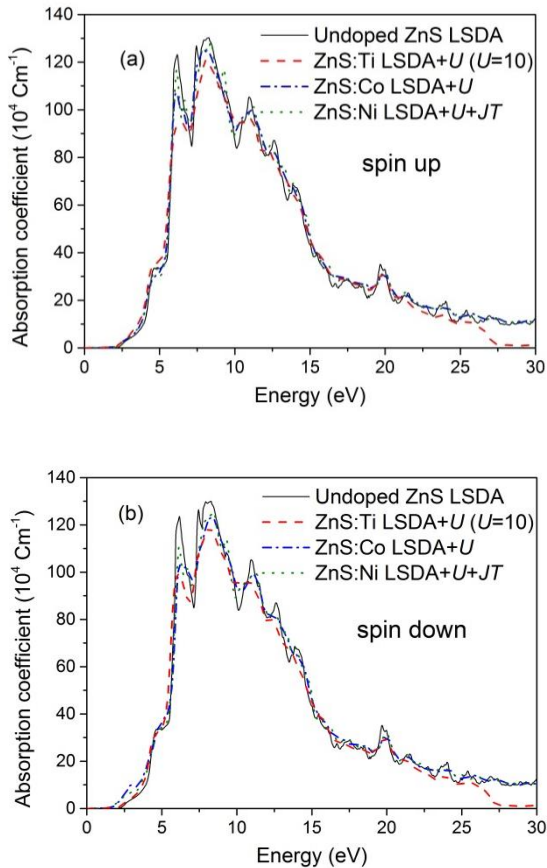


Fig. 9. The absorption coefficient of TM-doped ZnS for (a) spin up and (b) spin down channels

Tab .3 The non-magnetic optical band gap of TM-doped ZnS (E_{OG}).

ZnS:TM	Method	E_{OG} (eV) non-magnetic
Undoped ZnS	LSDA	2.110
ZnS:Ti	LSDA+U U=10 eV	2.028
ZnS:Co	LSDA+U U=3.3 eV	1.766
ZnS:Ni	LSDA+U+JT U=6.4 eV	1.603

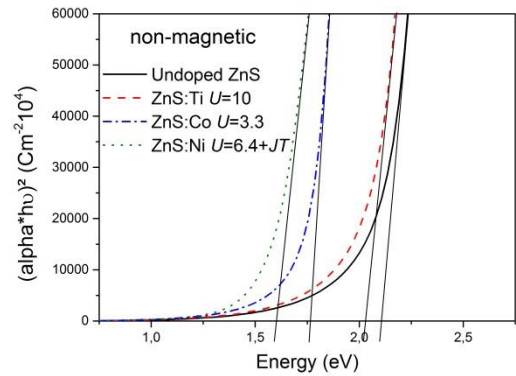


Fig. 10. $(\alpha \cdot hu)^2$ versus energy to calculate the energy band gaps of TM-doped ZnS

The optical parameters are important for the performance of new devices, especially for optoelectronics applications, renewable energy and solar cell technologies. The transition metals are one of the most effective dopant to tune optical, magnetic properties due to their abundant electron states. However, we calculate the dielectric constant $\epsilon(\omega)$, refractive index $n(\omega)$, and absorption coefficient $\alpha(\omega)$ of TM doped ZnS. We use the dielectric function to explain the linear response of these optical parameters to electromagnetic radiation, which is defined as $\epsilon(\omega) = \epsilon_1(\omega) + i\epsilon_2(\omega)$. The real part of dielectric function is reported in Fig. 6.a, in spin up, there are two localized peaks for pure ZnS at 4.19 eV and 5.60 eV. These peaks come mainly from the transition between S-3p of the valence band and Zn-4s of conduction band. While, the localized peak of pure ZnS at 5.87 eV disappeared after doping with TM impurity. Moreover, it is obvious that ZnS:Co and ZnS:Ni behave in the same way, maybe due to the nearest atomic number of Co ($3d^7 4s^2$) and Ni ($3d^8 4s^2$). Furthermore, the peak at 4.19 eV of pure ZnS was subdivided to two peaks, due to Ti dopant. The difference of spin polarization of the transition metals in the energy range between 0 eV to 6 eV allows a good conception of magneto-optics devices. The spin down channel of the real part of dielectric function is reported in Fig. 5.b. It can be seen that the material behaves differently to spin up. The peak localized at 4.19 eV is shifted to the lower energy for ZnS:Ti because the material is a n-type one. In addition, the $\epsilon_1(\omega)$ is negative between 7.43 eV to 13.16 eV. It is negative for pure ZnS and positive for TM-doped ZnS between 6.14 eV to 6.64 eV. The positive value of dielectric function means that photons propagate through the compound and when the dielectric function is negative, the electromagnetic wave is damped. Therefore, the imaginary part of dielectric function is reported in Fig. 7. In spin up, the main peak is at 6 eV and decreases by doping with transition metals. In spin down, the imaginary part of dielectric function behaves differently to spin up. Some intra-band transition are in the energy range between 0 eV and 3 eV which are explained by the electronic

transition found previously in the density of states. Therefore, it is noticed that the refractive index is linked to the real part of dielectric function. Fig. 8. shows the refractive index of TM doped ZnS in both spin directions. In spin up, the static refractive index $n(0)$ is 1.92, 1.93, 1.94, 1.94 for pure ZnS, ZnS:Ni, ZnS:Ti and ZnS:Co respectively. While, in spin down, $n(0)=1.92, 1.92, 1.98$ and 1.99 for pure ZnS:Ti, undoped ZnS, ZnS:Ni and ZnS:Co respectively. However, the static refractive index $n(0)$ of spin up is similar to that of spin down for undoped ZnS, while, it is different for doped ZnS. Furthermore, The absorption coefficient of TM-doped ZnS is reported in Fig. 9. In spin up, it can be seen the main absorption peak at 8.07 eV. It decreases from pure ZnS to ZnS:Co, ZnS:Ni and ZnS:Ti, respectively, due to TM mpurity. The absorption coefficient behaves in the same way in spin down channel. The main absorption peaks values of the absorption coefficient are located at energy range 8.15 eV. The good optical characteristics of ZnS:TM (TM= Ti, Co, Ni) are important for solar cells, photodetectors and optical sensors. ZnO:TM can be a good candidate for optoelectronics applications.

4. Conclusions

In summary, we calculated the electronic, magnetic and optical properties of transition metals doped ZnS. The band structure and the density of states calculations show that Ti-doped ZnS have a semiconducting behavior by using $U=10$ eV. That Hubbard value was found sufficient to obtain filled Ti-*d-eg* states. Co and Ni doped ZnS show spin polarization phenomenon with an insulating character in spin up and a metallic behavior in spin down. In contrast, by inclusion the Hubbard coulomb correction, ZnS:Co became half-metallc material with no spin polarization. Ni doped ZnS keeps its half-metallicity. In this case, we performed the calculation with the inclusion of the Jahn-Teller effect. That distortion, which breaks the cubic symmetry, removed the degeneracy of the Ni-*d-t2g* level, decreased the total energy of the system and opened up the band gap. Furthermore, the magnetic properties and the *sp-d* exchange couplings were calculated. The *p-d* hybridization mechanism dominates the ferromagnetic exchange interaction for ZnS:Ti and anti-ferromagnetic super-exchange interaction for ZnS:Co and ZnS:Ni. Therefore, we calculated the optical band gap of TM-doped ZnS. The optical band gaps was found to be decreased compared to the band gap of undoped ZnS. That tendency is in a good agreement with the experimental works [27-29]. Furthermore, the optical properties revealed a good quality of the TM-doped ZnS. The transition metals doped ZnS occurred new transition peaks in the real part and imaginary part of dielectric function. The main peaks of the absorption coefficient were found to be decreased when impurity effect was considered. This study confirms that TM-doped ZnS (TM=Ti, Co, Ni) can be a promising materials for the conception of optoelectronics devices.

Acknowledgements

The authors are highly grateful to ECP3M laboratory and the University of Mostaganem, Algeria for providing financial support.

References

- [1] M. Mall, L. Kumar, J. Lumin. **130**, 660 (2010).
- [2] A.A. Bol, J. Ferwerda, J.A. Bergwerff, A. Meijerink, J. Lumin. **99**, 325 (2002).
- [3] M. Nematollahi, X. Yang, U.J. Gibson, T. W. Reenaas. Thin Solid Films **590**, 28 (2015).
- [4] B. Poornaprakash, D. Amaranatha Reddy, G. Murali, N. MadhusudhanaRao, R.P. Vijayalakshmi, B.K. Reddy, J. Alloys Comp. **577**, 79 (2013).
- [5] M. S. Akhtar, M. A. Malik, Y. G. Alghamdi, K. S. Ahmad, S. Riaz, S. Naseem, Materials Science in Semiconductor Processing **39**, 283 (2015).
- [6] H. Q. Xie, L. J. Tang, J. L. Tang, P. Peng. Journal of Magnetism and Magnetic Materials **377**, 239 (2015).
- [7] H. Chen, D. Shi, J. Qi, B. Wang, Physica E **43**, 117 (2010).
- [8] Y. Huang, Z. Zhang, F. Ma, P. K. Chu, C. Dong, X. Wei. Computational Materials Science **101**, 1 (2015).
- [9] Y. Chen, W. Mi, J. Yang, Q. Song, H. Yan, T. Wei, Y. Guo. Solid State Communications **205**, 9 (2015).
- [10] H. Chen, P. Li, N. Umezawa, H. Abe, J. Ye, K. Shiraishi, A. Ohta, S. Miyazaki. The J. of Physical Chemistry **120** (10), 5549 (2016).
- [11] E. D. Bloch, M. R. Hudson, J. A. Mason, S. Chavan, V. Crocellà, J. D. Howe, K. Lee, A. L. Dzubak, W. L. Queen, J. M. Zadrozny, S. J. Geier, L. Lin, L. Gagliardi, B. Smit, J. B. Neaton, S. Bordiga, C. M. Brown, and J. R. Long. Journal of the American Chemical Society, **136**, 10752 (2014).
- [12] M. Saeed Akhtar, Saira Riaz, Shahzad Naseem, Materials Today: Proceedings. **2**, 5528 (2015).
- [13] S. Kumar, C. L. Chen, C. L. Dong, Y. K. Ho, J. F. Lee, T. S. Chan, R. Thangavel, T. K. Chen, B. H. Mok, S. M. Rao, M. K. Wu, Journal of Alloys and Compounds **554**, 357 (2013).
- [14] W. Fang, Y. Liu, B. Guo, L. Peng, Y. Zhong, J. Zhang, Z. Zhao, Journal of Alloys and Compounds **584**, 240 (2014).
- [15] M. S. Akhtar, S. Riaz, S. Naseem, Materials Today: Proceedings **2**, 5684 (2015).
- [16] H. Q. Xie, L. J. Tang, J. L. Tang, P. Peng. Journal of Magnetism and Magnetic Materials **377**, 239 (2015).
- [17] Y. Ohno, D. K. Young, B. Beschoten, F. Matsukura, H. Ohno, D. D. Nature **402**, 790 (1999).
- [18] R. Fiederling, M. Keim, G. Reuscher, W. Ossau, G. Schmidt, A. Waag, L. W. Molenkamp, Nature **402**, 787 (1999).
- [19] G. Kotliar, S. Y. Savrasov, K. Haule, V. S. Oudovenko, O. Parcollet, and C. A. Marianetti, Rev. Mod. Phys. **78**, 865 (2006).

- [20] T. Story, R. R. Galazka, R. B. Frankel, P. A. Wolff, Phys. Rev. Lett. **56**, 777 (1986).
- [21] S. Sanvito, P. Ordejon, N. A. Hill, Phys. Rev. B **63**, 165206 (2001).
- [22] C. Echeverria-Arrondo, J. Perez-Conde, A. Ayuela, Phys. Rev. B **82**, 205419 (2010).
- [23] H. Raebiger, A. Ayuela, R. M. Nieminen, J. Phys.: Condens. Matter **16**, L457 (2004).
- [24] T. Chanier, F. Virost, R. Hayn. Physical Review B **79**, 205204 (2009).
- [25] T. Mizokawa, A. Fujimori. Physical Review B, **56**, 11 (1997).
- [26] K. Osuch, E. B. Lombardi, W. Gebicki, Phys. Rev. B **73**, 075202 (2006).
- [27] R. Wang, H. Liang, J. Hong, Z. Wang. Journal of Photochemistry and Photobiology A: Chemistry, **325**, 62 (2016).
- [28] H. Xie, L. Tang, J. Tang, P. Peng. Journal of Magnetism and Magnetic Materials, **377** 239 (2015).
- [29] Y. F. Vaksman, Y. A. Nitsuk, Y. N. Purtov, A. S. Nasibov, P. V. Shapkin. I. I. Mechnikov Odessa National University, UDC 621.315.592 (2013).

*Corresponding author: aimouch.djamel@hotmail.com